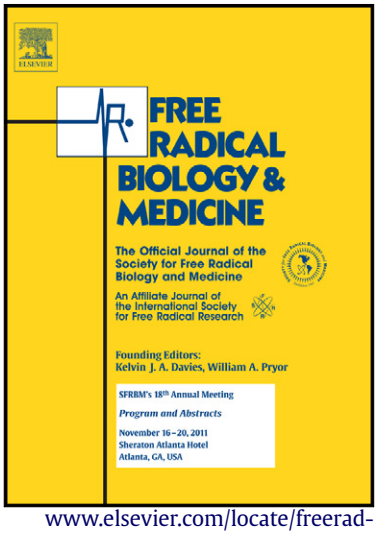

www.elsevier.com/locate/freerad-biomed

The role of strong hypoxia in tumors after treatment in the outcome of bacteriochlorin-based photodynamic therapy (PDT)

Martyna Krzykawska-Serda, Janusz M. Dąbrowski, Luis G. Arnaut, Małgorzata Szczygieł, Krystyna Urbańska, Grażyna Stochel, Martyna Elas

PII: S0891-5849(14)00210-X
DOI: http://dx.doi.org/10.1016/j.freeradbiomed.2014.05.003
Reference: FRB12012

To appear in: *Free Radical Biology and Medicine*

Received date: 8 January 2014
Revised date: 2 May 2014
Accepted date: 2 May 2014

Cite this article as: Martyna Krzykawska-Serda, Janusz M. Dąbrowski, Luis G. Arnaut, Małgorzata Szczygieł, Krystyna Urbańska, Grażyna Stochel, Martyna Elas, The role of strong hypoxia in tumors after treatment in the outcome of bacteriochlorin-based photodynamic therapy (PDT), *Free Radical Biology and Medicine,* http://dx.doi.org/10.1016/j.freeradbiomed.2014.05.003

The role of strong hypoxia in tumors after treatment in the outcome of bacteriochlorin-based photodynamic therapy (PDT)

Martyna Krzykawska-Serda,[a] Janusz M. Dąbrowski,[b*] Luis G. Arnaut,[c,d*] Małgorzata Szczygieł,[a] Krystyna Urbańska,[a] Grażyna Stochel[b] and Martyna Elas[a*]

[a]Faculty of Biochemistry, Biophysics and Biotechnology, Jagiellonian University, 30-387 Krakow, Poland

[b]Faculty of Chemistry, Jagiellonian University, 30-060 Krakow, Poland

[c]Chemistry Department, University of Coimbra, 3004-535 Coimbra, Portugal

[d]Luzitin SA, R. Bayer 16, 3045-016 Coimbra, Portugal

***Correspondence should be sent to** Dr. Janusz M. Dabrowski, jdabrows@chemia.uj.edu.pl, +48126632293, +48126340515 (fax), Prof. Luis G. Arnaut, lgarnaut@ci.uc.pt and Dr. Martyna Elas, martyna.elas@uj.edu.pl.

Abstract

Blood flow and pO_2 changes after vascular-targeted PDT (V-PDT) or cellular-targeted PDT (C-PDT) using 5,10,15,20-tetrakis(2,6-difluoro-3-N-methylsulfamoylphenyl) bacteriochlorin (F_2BMet) as photosensitizer, were investigated in DBA/2 mice with S91 Cloudman mouse melanoma, and correlated with long-term tumor responses. F_2BMet generates both singlet oxygen and hydroxyl radicals under NIR irradiation, which consume oxygen. Partial oxygen pressure was lowered in PDT-treated tumors and this was ascribed both to oxygen consumption during PDT and to fluctuations in oxygen transport after PDT. Similarly, microcirculatory blood flow changes as a result of the disruption of blood vessels due to the treatment. A novel non-invasive approach combining Electron Paramagnetic Resonance oximetry and Laser Doppler blood perfusion measurements allowed longitudinal monitoring of hypoxia and vascular function changes in the same animals, after PDT. C-PDT induced parallel changes in tumor pO_2 and blood flow, i.e., an initial decrease immediately after treatment, followed by a slow increase. In contrast, V-PDT led to a strong and persistent depletion of pO_2, although the microcirculatory blood flow increased. Strong hypoxia after V-PDT led to a slight increase of VEGF level 24 h after treatment. C-PDT caused a ca. 5-day delay in tumor growth, while V-PDT was much more efficient and led to tumor growth inhibition in 90% of animals. The tumors of 44% of mice treated with V-PDT regressed completely and did not reappear for over one year. In conclusion, mild and transient hypoxia after C-PDT led to intense pO_2 compensatory effects and modest tumor inhibition but strong and persistent local hypoxia after V-PDT caused tumor growth inhibition.

Keywords

Oxymetry, Blood flow, Vascular-targeted PDT, Bacteriochlorins, Hydroxyl radical, Singlet oxygen, Superoxide, Phototoxicity, Photodynamic therapy

Abbreviations

C-PDT, cellular-targeted photodynamic therapy; ER, endoplasmic reticulum; F_2BMet, 5,10,15,20-tetrakis(2,6-difluoro-3-N-methylsulfamoylphenyl) bacteriochlorin; PS,

photosensitizer; ROS, reactive oxygen species; NIR, near infrared radiation; VEGF, vascular endothelial growth factor, V-PDT, vascular-targeted PDT.

1. Introduction

Photodynamic therapy (PDT) is a clinically-approved therapy based on the destruction of neoplastic tissues [1], selective occlusion of choroidal neovascularization secondary to age related macular degeneration [2], and potentially useful to treat infection by multi-antibiotic resistant organisms [3]. It involves the use of photosensitizer, molecular oxygen and light of a specific wavelength in order to generate reactive oxygen species (ROS, namely singlet oxygen and hydroxyl radicals) which cause apoptosis, autophagy or necrosis of the treated cells, the closure of the blood vessels and eventually an activation of anti-tumor immune response [4]. Thousands of photosensitizers have been tested *in vitro* and *in vivo* but only a few of them managed to reach clinical trials [5, 6]. The simultaneous fulfillment of all of criteria for ideal photosensitizer is extremely difficult, and the heterogeneity of pathologically altered tissues and their different interaction with the photosensitizer are additional challenges that must be addressed by the therapy. Recent advances in PDT suggest that a class of compounds that meet most of the requirements for ideal PDT agents are bacteriochlorin derivatives [7-22]. They are characterized by a very high molar absorption coefficients ($\varepsilon \geq 100\ 000\ M^{-1}\ cm^{-1}$) in the therapeutic window and therefore may be effective at lower concentrations and allow for a deeper penetration of light in tissue when compared to porphyrin derivatives. Recently, new synthetic bacteriochlorins attained the photostability, long lifetimes in the excited triplet states and high quantum yields in the generation of ROS, that are desirable for PDT photosensitizers. Moreover, some of them display low dark cytotoxicity, high phototoxicity, amphiphilicity and high accumulation in sensitive organelles such as the endoplasmic reticulum (ER) and mitochondria. In particular, in the family of halogenated sufonamide bacteriochlorins it was possible to identify a photosensitizer, 5,10,15,20-tetrakis(2,6-difluoro-3-*N*-methylsulfamoylphenyl)bacteriochlorin (F_2BMet, illustrated in **Scheme 1**) that closely

matches the properties of an ideal PDT photosensitizer and proved very efficient *in vitro* and *in vivo* [23, 24].

A properly designed photosensitizer may not have the expected therapeutic success if it is not used with an appropriate protocol. For example, PDT exerts a profound effect in the tumor tissue oxygenation level and the generation of ROS during the therapy may lead to depletion of oxygen in the tumor, which may impair the efficacy of the therapy [25, 26]. In order to avoid that oxygen consumption becomes a limiting factor in PDT, various authors proposed the fractionation of light irradiation, with short dark periods (150-200 s), to allow for tissue re-oxygenation [27-30]. Furthermore, tumor tissue oxygenation exhibits very heterogeneous response to PDT, both spatially in different tumors [31], and between tumors [32]. For photosensitizers that have the vasculature as the main target [30, 33, 34], the supply of oxygen to tissue might be limited due to vascular damage resulting from PDT. Occlusion of blood vessels and, in consequence, hypoxia can occur within a few minutes after the beginning of PDT. This effect may be reversible or irreversible, depending on the amount of the photosensitizer present in tissue and applied light dose. Even if vessels stay intact and their function remains unchanged immediately after treatment, irreversible vascular damage and collapse develops within hours, leading to hemorrhage and tissue necrosis. The expected decrease in tumor oxygenation, or increase in hypoxia, was observed in vascular-targeted PDT [27, 30, 35]. On the other hand, when tumor cells are targeted in PDT, limited oxygen consumption can lead to increase in oxygenation due to decrease in metabolic consumption of oxygen by cells [36]. Thus, understanding tumor tissue oxygenation before, during and after PDT is useful to obtain the optimal parameters for therapy, and it has even be suggested that monitoring of PDT-induced changes in tumor oxygenation may be a valuable prognostic indicator [37]. One of the indirect methods of hypoxia detection is assessing the presence of protein associated with, or induced by, hypoxia such as VEGF [38, 39].

Accurate estimation of hypoxia *in vivo* remains a challenge, although various methods have been tested *in vivo*, such as pimonidazole retention or hypoxia-induced protein staining [40]. Remarkably, electron paramagnetic resonance (EPR) oxymetry allows for repetitive and non-invasive oxygen measurements in tumors of living animals

[41-44]. In particular, solid oxymetric microcrystals such as lithium phthalocyanine (LiPc) bring accurate and precise information on oxygen partial pressure in probe surroundings [45-46]. Likewise, optical methods, e.g. Laser Doppler Perfusion Imaging (LDPI), give access to non-invasive blood flow measurements. LDPI provides information on microcirculation of the surface tissues (up to mm) from the tumor surface and tumor surrounding area. Combining the two methods gives insight into tissue physiology in the local (EPR) and global (LDPI) scale, and provides the grounds to understand the roles of vasculature, microcirculatory blood flow and pO_2 in the outcome of PDT. **Scheme 2** illustrates how both techniques were implemented in this study. As both methods are non-invasive, longitudinal studies on hypoxia and vascular function may be performed in the same animals. The goal of this study is to determine pO_2 and blood flow changes after vascular PDT (V-PDT, with a drug-to-light interval of 15 min) and tumor-cell targeted PDT (C-PDT, with a drug-to-light interval of 72 h) using a bacteriochlorin derivative and estimate how they correlate with therapy efficacy. *In vivo* measurements of pO_2 in the tumor give estimates of the oxygen consumption changes during PDT, as well as of changes in its transport and metabolic consumption after PDT. Simultaneous measurements of microcirculatory blood flow reveal the disrupted function of blood vessels after PDT. Altogether, these experiments may verify the hypothesis that V-PDT massively destroys tumor vessels and leads to extreme hypoxia within the tumor, whereas tumor-targeted C-PDT preserves the oxygenation level in the tumor.

2. Materials and methods

2.1.Chemicals

5,10,15,20-Tetrakis(2,6-difluoro-3-N-methylsulfamoylphenyl)bacteriochlorin (F_2BMet or LUZ11) [23] was provided as a powder in sealed vials under protective atmosphere by Luzitin SA (Coimbra, Portugal). Solutions for intravenous (i.v.) administration were prepared by dissolving the desired amount of F_2BMet in a certain volume of Cremophor EL – CrEL – (Sigma, Germany) mixed in 1:1 (v/v) proportion with ethanol 99.8% (POCH, Poland), followed by dilution by a factor of 50 with 0.9% NaCl aqueous solution, and then injection in the animals [24]. F_2BMet is readily soluble in CrEL:ethanol, which forms micelles when added to the saline solution. This

administration vehicle is well tolerated and prevents the precipitation of the photosensitizer in the organism. The concentration of F_2BMet in the administration vehicle was 200 mg/L. The F_2BMet dose used in all animals was 2 mg/kg body weight, assuming a pure starting material. Medium for cell culture (RPMI, F10) and PBS (phosphate-buffered saline) were purchased from Biomed, Poland. Trypsin/EDTA, cell culture media and supplements, and animal serum were purchased from Biochrom (Berlin, Germany). Butorphanol (Butomidor) was obtained from Richter (Pharma AG, Wells, Austria). Medetomidine hydrochloride (Cepetor, ScanVet, Warszawa, Poland) and ketamine (Bioketan, Biowet Pulawy, Poland) were used as anesthetics during *in vivo* experiments.

2.2. Absorption and fluorescence spectra

UV/VIS absorption spectra were recorded in quartz cuvettes with Shimadzu 2100 spectrophotometer. Fluorescence studies were carried out using a Luminescence Spectrometer LS 50B (Perkin–Elmer).

2.3 Tumor model

S91 Cloudman mouse melanoma cell line (subline I3) was described previously [19-21]. The cells were grown as monolayers in the RPMI medium, supplemented with 5% fetal calf serum and antibiotics (penicillin, streptomycin) at 37 °C in a humidified atmosphere containing 5% CO_2, as described elsewhere [47-48]. Shortly before tumor inoculation, cells were washed with PBS and harvested by trypsynization. After centrifugation cells were washed again with warm PBS, and 0.5 $\times 10^6$ of cells were administered intradermally in 0.05 ml into the hind right leg of DBA/2 mice. The tumors grew visible 7-10 days after implantation and their volumes (V) were estimated on the basis of their three perpendicular diameters according to formula: $V= \pi/6(a\times b\times c)$, where a, b, and c stand for the respective perpendicular diameters of the tumor.

2.4 Animal model and experimental groups

Male DBA/2 mice, implanted with the Cloudman S91 melanoma, were 3-4 months old and about 25 g each. The mice were kept on a standard laboratory diet with free access to drinking water in community cages and a 12 h day/night regime. The animals

used in the present study were obtained from the animal breeding facility at Mossakowski Medical Research Centre Polish Academy of Sciences, Warszawa, Poland. Before the experiments animals were quarantined for 2 weeks. The use of these animals for experimental purposes was approved by the Jagiellonian University Committee for Ethics of Experiments on Animals (permission no. 114/2009, 76/2011 and 42/2014).

In order to make possible measurements of pO_2 and blood flow at the same time point, two separate sets of animals were used. Within each set the animals were divided into the following experimental groups: (a) V-PDT: light irradiation given 15 min after PS injection, (b) C-PDT: light irradiation given 72 h after PS injection, (c) light control - animals treated with carrier for PS and light only, (d) dark control - animals treated with PS only, without light. Randomly chosen animals were euthanized at certain time points for other tests, and all the remaining mice were observed for survival and acute effects, such as erythema and edema.

2.5 Biodistribution experiments

The i.v. administration of the drug formulation was done when the tumor attained a volume of 30-60 mm^3 in each animal, which usually took 10 days after the inoculation. The formulation, corresponding to a 2 mg/kg of F_2BMet, was slowly injected in the tail vein of each animal, and the biodistribution was evaluated at 2 time points after administration: 15 min and 72 h. At the selected time points post injection, the mice were anesthetized with ketamine and xylazine. For each animal, the following organs and tissue samples were collected separately and weighed: tumor, muscle, skin, liver, spleen, kidneys, intestines, heart, lungs and blood. The content of F_2BMet in the tissue samples was determined by fluorescence measurements. In order to extract the pigments, tissue samples were separately homogenized in 1 ml of ice-cold solution ethanol:DMSO (75:25) during 1 min, using a tissue homogenizer Di25 basic, IKA-Werke, GMBH&Co (Stauten, Germany). The homogenate was centrifuged at 1800*g* for 1 min at 5 ºC, the supernatant was collected and the pellet was re-extracted 3 more times using the procedure described above, to ensure a complete recovery of the drug. The extracts were pooled and the final volume adjusted to 5 ml. The fluorescence analysis of the extracts was done less than 3 h from the harvest. The samples were excited at 505 nm and the

fluorescence spectra were recorded in the range between 600 and 800 nm. The amount of F_2BMet in the tissues is reported as the average from 5 animals, with the standard error of the mean (SEM).

2.6 PDT treatments

When the tumors reached a volume of 30-50 mm^3, an appropriate volume of a freshly prepared F_2BMet drug formulation was administered i.v. in each mice to give at a dose of 2 mg/kg body weight. Before the PDT treatment, animals were given subcutaneously (s.c.) butorphanol at a dose 3 mg/kg (Butomidor, Richter Pharma AG, Wells, Austria) to alleviate the pain and then anaesthetized by i.p. injection of the mixture of 0.1 mg/kg medetomidine hydrochloride (Cepetor, ScanVet, Warszawa, Poland) and 50 mg/kg of ketamine (Bioketan, Biowet Pulawy, Poland). During the anesthesia the animals were kept at stable temperature around 35 °C using heating pad.

Two types of PDT protocols were tested: vascular-targeting V-PDT (15 min time interval between PS and light administration), and tumor cellular-targeting C-PDT (72 h interval between PS and light administration). In all cases the tumors were irradiated from distance of 1 cm for 30 minutes using a 750 nm laser light at a final dose of 86 J/cm^2. As a light source a 750 nm Hamamatsu diode laser LA0873 with power supply ThorLab 500 mA ACC/APC was used. We selected a low laser fluence rate for this study, 48 mW/cm^2, which is less than half of that typically used in PDT, to minimize heterogeneous oxygen depletion during the irradiation. A laser power meter (Field MaxII-TO, Coherent, Portland, USA) was used to monitor the light power.

2.7 ROS detection

The 3'-p-(aminophenyl)fluorescein (APF), a probe with higher selectivity towards hydroxyl radicals, and Singlet Oxygen Sensor Green® (SOSG), a probe specific for singlet oxygen, were employed for detection of ROS in aqueous solutions during illumination. APF reacts preferably with hydroxyl radical to produce fluorescein, which emits at 530 nm when excited at 488 nm. SOSG reacts very specifically with singlet

oxygen to generate a fluorescent endoperoxide that emits at 525 nm when excited at 505 nm. Bacteriochlorin solutions in DMSO were diluted to a final concentration of 5 μM per well in PBS (final [DMSO] ≈ 0.4%). Next, the probes SOSG or APF were added to each well to a final concentration of 10 μM. The solutions were irradiated using the same light source as for PDT treatment for various time intervals up to 30 minutes, which correspond to a maximum dose of 86 J/cm^2 at 48 mW/cm^2. The microplate reader (Tecan Infinite M200 Reader) was used for acquisition of fluorescence signal from the probes immediately before and after each illumination period. When APF was employed, fluorescence emission at 515 nm was measured upon excitation at 490 nm. With SOSG, the corresponding emission and excitation wavelengths were 525 and 505 nm, respectively. The wells were always exposed to air and oxygen depletion in the solution is unlikely to occur at the low fluence rate used in this experiment.

2.8 Tumor pO_2 measurement

Crystalline oxymetric probe lithium phthalocyanine (LiPc, a gift from Prof. Harold Swartz, EPR Center, Dartmouth Medical School, Dartmouth, USA) was inserted into the S91 Cloudman melanoma tumor growing in the right hind leg of DBA/2 mice. Approximately 0.1 mg of LiPc in crystal form was implanted per mouse. No side effects, such as inflammation, redness, edema, or morphological changes (as detected by ultrasonography) were observed after LiPc implantation. The EPR measurements started 3 days after LiPc implantation (see Fig. S1 in the Suplementary Materials) to allow for its stabilization in the tissue [49-50]. Mice under anesthesia were placed in an animal holder, with the right hind leg perpendicular to the mouse support. The mouse leg was placed closely to the surface of the coil. The leg was immobilized carefully making sure that blood flow was not perturbed. EPR spectra were taken using the following parameters: microwave frequency 2.13 GHz (S-band), microwave power 4 mW, sweep field 5 G, gain 2×10^5, modulation amplitude 0.08 G, time constant 300 ms, sensitivity 10 mV. For a single measurement 3 scans, 512 s each, were taken and averaged. The pO_2 was determined from the linewidth of the EPR spectrum of the LiPc signal. EPR Fitting Software v3.0.2K (obtained from dr. Ben Williams and Tom Matthews, EPR Center, Dartmouth Medical School) was used to fit the linewidth of the LiPc signal. The linewidth was then recalculated for pO_2 using the calibration curve, obtained from spectra

of LiPc crystal in different gaseous mixtures, using a coefficient of 5.79 ± 0.42 mG/mm Hg (in the range between 0 and 56 mmHg).

2.9 Blood perfusion measurements

Laser Doppler Perfusion Imaging (LDPI) is a noncontact laser imaging technique for the measurement of superficial blood perfusion. Blood perfusion was measured with a LDPI Periscan system II (Perimed AB, Järfälla, Sweden) before, 15 min and 3 h after the treatment and then every 24 h for several consecutive days. The skin on the leg with the tumor was scanned with pulsed laser light (670 nm, 1 J maximal output power). Photons that are dispersed by moving blood cells undergo a change in wavelength/frequency (a Doppler shift), while photons that encounter static structures return with the same frequency to the detector. The perfusion can be calculated since the magnitude and frequency distribution of the Doppler-shifted light are directly related to the number and velocity of blood cells but unrelated to their direction of movement. Penetration depth is around 0.5-1 mm according to the manufacturer. The color images of the microcirculatory perfusion results are expressed as arbitrary units, and the scanning system is calibrated before each set of measurements using the motility standard provided. For quantitative analysis, raw read-out data (in V) from the tumor area were presented as a histogram (using Image J software). Microcirculatory blood perfusion was expressed as the ratio between median blood flow measured in the tumor area to that measured in the same region in normal contralateral leg. Likewise, measurement of perfusion in the area of *vena saphena lateralis* in the tumor leg was referenced to the same area in the normal leg. This eliminates differences in blood perfusion, such as temperature, anesthesia level and the general mouse condition. For a single animal median values of blood flow were calculated with SD and for a group of animals values were calculated as weighted means of medians with SEM.

2.10 PDT induced edema and erythema in the treated legs

Edema was expressed as tumor volume relative to stage before treatment. Erythema was evaluated on the scale between 0 and 2, with 0 – no erythema, 0.5 - minor, 1 – moderate, 2 – intense erythema.

2.11 Processing the samples and VEGF ELISA assay

Whole tumors were isolated 24 h after illumination and stored in liquid nitrogen no longer than 2 days. The samples (17 ± 3 mg) were homogenized (30-times) in 100 µl ice-cold PBS. An additional 100 µl of ice-cold PBS was added and samples were sonicated for 5 min in room temperature. Homogenized samples were centrifuged at 10,000 rpm for 10 min in 4 °C. The supernatants were collected and concentration of protein was measured by the Bradford method. All samples were stored at -24°C for less than 1 day. Quantitative sandwich enzyme immunoassay for VEGF (ELISA assay) was performed according to manufactured protocols (R&D, MMV00). In each well 20 µg of total protein was added. Each tumor sample was prepared as duplicate.

2.12 Ultrasonography

An ultrasonographic imager Vevo 2100 (VisualSonics, Toronto, Canada) was used for obtaining the images of tumors and localization of LiPc crystals (B-mode). Doppler-mode was used to images density of vasculature near oxygen spin probe (0.25 mm radius around LiPc). Vevo 2100 1.2.0 software was employed for tumor and LiPc delineation.

2.13 Statistical analysis

Group mean values of pO_2 and blood flow were calculated as weighted means, with variance as weights. Statistical significance was determined by Student t-test, Welch t-test, U-test or Fisher test. Kaplan-Meier statistical significance was determined using Wilcoxon analysis. Regression coefficients were determined using "fit linear" Origin routine and Statistica, with errors as weights, when possible. Histograms of blood perfusion values were analyzed using matrices of perfusion values expressed in absolute values measured [V]. Only tumor area pixels were included in histograms. Difference between tested groups was accepted as significant for $p<0.05$ or as described in figures captions.

3. Results

3.1. Spectroscopic properties of F_2BMet in the administration vehicle

F_2BMet exhibits the characteristic bacteriochlorin absorption spectrum with a broad near-UV Soret feature with two peaks, a near-infrared Q_y band of comparable intensity and only a narrow band in the green (≈510 nm). Representative spectra recorded in the

vehicle used for i.v. injections in animals *in vivo* studies are shown in **Figure 1.** The $Q_y(0,0)$ absorption maximum of F_2BMet is at 748 nm in the vehicle, and the $Q_y(0,0)$ fluorescence peak is bathochromically shifted by 2 nm. The vehicle used in the *in vivo* experiments contains CrEL:ethanol:NaCl 0.9% in a 1:1:98 (v/v/v) proportion. The infrared absorption coefficient of F_2BMet dissolved in this formulation (ε_{max}=125 000 M^{-1} cm^{-1}) is smaller than in ethanol (ε_{max}=140 000 M^{-1} cm^{-1}) [23]. A bacteriochlorin with molar absorption coefficient in excess of 100 000 $M^{-1}cm^{-1}$ in this formulation is evidence for the absence of aggregation and enables the efficient use of F_2BMet at much lower concentrations than its porphyrin and chlorin analogues. Moreover, light at 748 nm penetrates deeply into human tissues without any side effects.

3.2. Overview of blood flow and oxygenation in tumors

Figure 2 shows that blood perfusion on the surface of untreated tumors is heterogeneous. The histograms of blood perfusion display a wide variety of distributions, with examples of wide, narrow, single-or double-peaks. Apparently, heterogeneous microcirculation networks already exist in untreated tumors. **Figure 3** shows images of the superficial microcirculatory blood flow in the leg of mice with and implanted S91 tumor, before PDT and 15 min, 3 h or latter times after V-PDT or of C-PDT. Shortly after V-PDT the blood perfusion is decreased, and then a gradual increase up to the maximum on day 7 is observed (**Figure 3A, B, 3.1**). The increase in blood perfusion after C-PDT (**Figure 3 C, D, 3.2**) attains a higher value than after V-PDT in the same time scale.

Figure 4 presents representative changes in pO_2 observed for animals subject to V-PDT and C-PDT. It is very striking that the tissue pO_2 level recorded immediately after V-PDT, and for at least the subsequent 24 h, decreased to nearly zero (**Figure 4.1**). A slight increase in pO_2 was later observed in one animal, reaching 10 mmHg in day 4 (**Fig. 4.1A**), but the pO_2 value in the other animal did not recover in the observation time (**Fig. 4.1B**). In contrast, C-PDT led to a transient decrease in pO_2, lasting usually no more than 3 h, followed by a recovery of pO_2. In one animal, the tumor tissue pO_2 increased even up to 35 mm Hg (**Fig. 4.2D**), which is much higher than the value before PDT. The ultrasonographic images of individual animals show sagittal slices of murine legs with tumor cross section delineated in green and position of oxymetric spin probe LiPc

marked in red (**Fig. 4A-D**). Analysis of all tumors indicated that there was no relationship between LiPc position within the tumor and pO_2 reading, i.e. the depth of the probe location in the tumor does not determine the pO_2 reading (compare Figures S2 and S3 in the Supplementary Materials).

Figure 5 presents the mean pO_2 and blood flows of V-PDT and C-PDT treated animals, as well as of control groups. V-PDT and C-PDT protocols lead to statistically significant differences in tumor pO_2 values. Surprisingly, both protocols led to a strong stimulation of blood flow 2 days after the treatment, which was sustained for two weeks in the case C-PDT.

3.3. C-PDT, but not V-PDT induced parallel changes in tumor pO_2 and blood flow

A slight reduction in pO_2 was noted immediately after V-PDT, which was partially recovered in the following 24 hours, and then deceased to baseline values (**Fig. 5A**). In contrast, blood perfusion decreased in the first 24 h after V-PDT, and then increased from day 2 to day 7, to a value 8 times higher than at day 1.

The mean pO_2 in tumors treated with C-PDT strongly decreased immediately after illumination (from 3 mmHg to 0 mmHg), but then increased up to 12 mmHg at 72 h and remained high. The mean blood flow did not change in the first 24 h after C-PDT, and then gradually increased up to a maximum perfusion 5 times higher on day 9. Both pO_2 and blood flow exhibited similar pattern of changes in C-PDT, namely a pronounced increase after PDT and high values one week after PDT. However, the fast reduction in pO_2 immediately after illumination is not associated with a corresponding blood flow change (**Fig. 5B**).

Maximal blood perfusion in tumors was reached 7 to 9 after PDT for both protocols, and was 8 and 5 times higher for V-PDT and C-PDT than for a normal leg, respectively. Both protocols led to an initial decrease in pO_2. However, on average, V-PDT decreased pO_2 from 2 to 1 mmHg and maintained pO_2 below 2 mmHg in the first 3 days after PDT, whereas C-PDT depleted pO_2 from 3 to 0.5 mmHg but then it increased up to 12 mmHg in the third day after PDT. Both pO_2 and blood flow control values were changed slightly

in the dark (**Fig. 5D**), whereas an increase up to 6 mmHg in pO_2 value was observed after illumination (**Fig. 5C**).

3.4 Vascular targeted PDT enhances VEGF level

Figure 6 shows that the VEGF levels were slightly increased in tumors 24 hours after V-PDT, but not after C-PDT. This parallels pO_2 depletion and strong hypoxia in tumor tissue after V-PDT (**Fig. 5**). It is worth noticing that distribution of this protein content was skewed in all groups suggesting high heterogeneity in VEGF level. However, in V-PDT group VEGF distribution became normal, indicating more homogenous response.

3.5 Biodistribution of F_2BMet after 15 min and 72h post injection

The biodistribution of F_2BMet were studied after the administration in the tail vein of DBA/2 mice of a drug dose of 2 mg/kg in 0.1 ml of vehicle. The solvent mixture employed was CrEL:ethanol:NaCl 0.9% in a 1:1:98 (v/v/v) proportion. F_2BMet is very soluble in this vehicle, and the solvent mixture was not toxic to the mice. Five animals per group were sacrificed at different time points (15 min and 72 h post injection) and F_2BMet was extracted from the target tissues, including tumor, muscle, skin, liver, kidneys, heart, lungs, spleen and blood. Figure S4 in Supplementary Materials shows representative fluorescence spectra of F_2BMet extracted from tumor, muscle and skin 72 h after i.v. injection. The largest concentrations of F_2BMet, in terms of μg of F_2BMet per g of wet tissue, after 15 minutes from injection were observed in the blood, spleen, lungs, tumor and liver and are presented in **Table 1**. Interestingly, 72 hours after F_2BMet injection its concentration in tumor increased to more than 5 μg per 1 g of wet tissue and was the highest amount among all studied organs/tissues. The tumor-to-skin (T/S) and tumor-to-muscle (T/M) ratios at this time point are 3.8 and 4.3, respectively. Tumor to surrounding tissues ratios after 15 min and 72 h are collected in **Table 2**.

3.6 Photodynamic efficacies after V-PDT and C-PDT

Figure 7 shows Kaplan-Meier plot with percentage of animals with local tumor control, i.e. tumor volume less than 400 mm^3. Half of animals survived until day 10 in

controls, day 16 after C-PDT, whereas after V-PDT 50% were still alive on day 47. In this group of animals in 44% of mice tumor regressed and did not reappear for 1 year (the end of observation time). This high photodynamic activity towards very resistant melanoma tumors may be explained by efficient generation of both singlet oxygen and hydroxyl radicals. **Fig. 8** shows that F_2BMet activates both APF and SOSG, but the saturation of the fluorescein signal occurs at a lower light dose than that of the endoperoxide. This is assigned to a faster consumption of APF, which would be consistent with the ability of F_2BMet to generate both hydroxyl radicals and singlet oxygen under illumination in biological media [23], that would react with APF to release fluorescein, as opposed to SOSG that reacts selectively with singlet oxygen. The hydroxyl radical is a most cytotoxic species and is expected to be a major contributor to tumor damage in PDT with F_2BMet.

The kinetics of the tumor growth of individual animals is presented in Supplementary Figure S5. Some acute reactions to PDT treatment were observed, such as edema and erythema at the illuminated site. Erythema usually appeared on day 2, attained its maximum at day 3, and lasted until day 5-6. Interestingly, erythema was present in fewer animals after V-PDT than after C-PDT (**Fig. 9A**). Edema of the leg with the tumor was maximal at 3 h after V-PDT, reaching a volume 30 times higher than before the treatment, and then decreased up the day 4 (**Fig. 9B**). The maximal edema in animals treated with C-PDT was 15 times higher than the tumor volume before the treatment at day 1, but significantly smaller than the maximal edema observed with V-PDT (**Figure 9B**). The gradual increase of volume seen in the light control reflects the tumor growth (**Fig 8B**).

Figure 9C shows changes in relative blood flow after PDT in the region of the *vena saphena lateralis*. A gradual decrease in blood flow in the first 24 h was seen both after V-PDT and C-PDT. After C-PDT the blood flow returned to the normal level within 3-4 days, whereas after V-PDT the strong inhibition of blood flow was maintained for 4 days and suddenly returned to the normal level on day 5.

4. Discussion

We have recently shown that when halogenated and sulfonated bacteriochlorins absorb NIR radiation, they generate high amounts of singlet oxygen and superoxide ion

radicals and, subsequently, hydrogen peroxide and hydroxyl radicals [12]. The combined effects of singlet oxygen and hydroxyl radical make bacteriochlorins more promising and effective in PDT than the corresponding chlorins [51-52]. Exchanging sulfonic to sulfonamide groups resulted in an even more significant enhancement of photocytotoxicity *in vitro* [20] and *in vivo* [21]. The earlier saturation of the signal generated by APF with respect to that generated by SOSG, shown in **Fig. 8** for the same concentrations and fluence rates, is consistent with the generation of large quantities of both singlet oxygen and hydroxyl radicals when F_2BMet is illuminated, because SOSG reacts only with singlet oxygen but APF can be consumed in reactions with hydroxyl radicals and singlet oxygen. The conditions employed in Fig. 8 are similar to those of *in vivo* experiments (the same light source, fluence rates and light doses). A recent study comparing V-PDT and C-PDT protocols with F_2BMet in BALB/C mice with subcutaneously implanted CT26 cancer cells showed that V-PDT could lead to a higher rate of tumor remissions than C-PDT [24]. **Fig. 7** shows that V-PDT also leads to better treatment outcome than C-PDT in a different tumor model. In addition to these extensions of previous work, we now report for the first time non-invasive EPR oximetry and LDPI measurements that unravel the underlying reasons for the difference between V-PDT and C-PDT.

Non-invasive measurements of tumor pO_2 (EPR) and microcirculatory blood flow (LDPI) provide complementary views on physiology of the vasculature after treatment. Moreover, they give information both on the local (tumor area around the LiPc probe) and on the global (superficial microperfusion of the tumor and surrounding areas) scales. Earlier studies on tumor pO_2 after PDT suggested that different patterns in pO_2 and blood flow could emerge after V-PDT or C-PDT [53-55]. A strong depletion in pO_2 and blood flow should be expected after V-PDT, whereas C-PDT was anticipated to produce a temporary increase in pO_2. However, the patterns emerging from our studies are more intricate.

V-PDT is an effective therapeutic approach using an array of photosensitizers [24, 30, 34, 55]. It aims at the destruction of tumor vessels, limiting the tumor nutrition and controlling tumor growth. In V-PDT light is applied very soon after the photosensitizer administration, while it is still within the vascular compartment. Alternatively, in tumor

cellular-targeted PDT (C-PDT), the drug-to-light interval is increased to take advantage of the accumulation of the photosensitizer in tumor cells and of its faster clearance from normal tissues. C-PDT aims at the selective destruction of the tumor tissue while sparing the normal tissues. Biodistribution studies have demonstrated that tumor-to-muscle or to skin tissue ratios peak at 24-72 h post-i.v. administration of the photosensitizer [21, 24, 45], and in this work we performed C-PDT at 72 h post-i.v. administration of F_2BMet when the tumor-to-muscle ratio attains 4.3.

PDT caused changes in tumor pO_2 and microcirculation blood flow that are specific to each protocol. V-PDT led to a decrease in pO_2 for up to several days, indicating deep and long-lasting (chronic) hypoxia. A slight increase in VEGF level 24 h after V-PDT indirectly confirms hypoxia induced by the therapy. However, the decrease in pO_2 after C-PDT lasted for only a short period of time and was followed by a large increase in pO_2 that lasted for 4-5 days after therapy. The decrease right after therapy might be explained by consumption of oxygen during PDT. The increase in pO_2 to 6 mmHg at 3 h post-PDT, and then to 10 mmHg at 24 h post-PDT, probably results from compensatory delivery of oxygen due to previous consumption during long time of irradiation (30 min) as it is illustrated in **Fig. 9A**. C-PDT effectively destroys tumor cells (histology, data not shown), leading to decreased oxygen metabolism, and this may allow the high pO_2 levels to last for several days. Tumor regrowth started around day 5, which correlates with decrease in pO_2 level observed henceforward.

The question arises as to the influence of these effects on the therapeutic outcome. **Figure 10A** expresses the decrease in pO_2 due to therapy, Δ(before–immediately after), as a function of the increase in pO_2 within 24 h after the treatment, Δ(24h–15min). This reveals that in C-PDT these pO_2 levels are correlated (R^2=0.84), i.e., the oxygen consumption during PDT evokes a compensatory response leading to an increase in pO_2 post-PDT. Such a correlation was not found for V-PDT, where the decrease in pO_2 post-PDT did not recover, and suggests an almost complete destruction of the vasculature. **Figures 5A and 5B** show that V-PDT produces chronic hypoxia in the tumor, and the Kaplan-Meier plot in **Figure 7** show that this is critical for the therapeutic outcome of PDT.

The value of pO_2 in the tumors immediately after V-PDT correlated with efficacy of the therapy regarded both as tumor volume on day 5-7 (R^2=0.71, p=0.02) and time-to-tumor volume of 400 mm^3 (R^2=0.77, p=0.01). For C-PDT no such correlations were found. It is worth noticing that neither changes in blood flow, Δ(24h–15 min), nor in ΔpO_2 , Δ(before- immediately after), correlated with therapeutic efficacy. Rather than the variation in pO_2, it is the absolute values of pO_2 (0-1 mm Hg) that determines the efficacy of V-PDT (**Fig. 10B**). Minimal pO_2 after PDT correlates with lifetime of animals (N=7, R^2=0.76, p=0.047). This corroborates the conclusions that strong local hypoxia due to therapy is required to inhibit the tumor growth and increase life expectancy.

We suggest that the existence of a very strong hypoxia (0 mmHg, **Fig. 9B**) is a good predictor of the therapy outcome. Partial dysfunction of the blood flow does not guarantee a good long-term tumor response to PDT and, conversely, might even have a stimulatory effect on tumor growth (especially with simultaneous increase in VEGF in the surrounding tissue). An increase in blood flow due to C-PDT on day 5-7 correlated with tumor volume the same day (the higher the increase in blood flow, the bigger the tumor) (R^2=0.58, p=0.0025). This suggests that some destruction of blood microcirculation occurs in C-PDT, and that it stimulates tumor growth (Fig. S5 in the Supplementary Materials).

Interestingly, both V-PDT and C-PDT stimulated superficial tumor blood flow when compared with controls (**Fig. 5A-D**). This may be a consequence of either scab healing and/or local inflammation, evidenced by edema and erythema, and it is uncertain whether the increased microcirculation has any effect on tumor growth. Edema was much more pronounced after V-PDT than after C-PDT. The source of interstitial edema might be leakage from vessels or a sign of immune response. Leakage from destroyed vasculature should be expected after V-PDT. However, edema correlated with time-to-tumor volume of 400 mm^3 for animals treated with C-PDT (data not shown) but not for V-PDT, which suggests that inflammation or low vasculature leakage might have a stimulatory effect on tumor growth. Edema of the tumor leg might disturb the blood perfusion and pO_2 measurements because the larger volume of fluid present in the tissue might lead to larger distances to vessels (almost twice, [56]). However, minimal blood flow was recorded at 24h after V-PDT while maximal edema was observed at 12h,

indicating that edema is not biasing our blood flow measurements. Moreover, blood flow measured in the area of *vena saphena lateralis* was maintained at very low levels for 4 days, while edema was gradually decreasing. The influence of edema in blood flow measurements after C-PDT cannot be excluded. On the other hand, the stronger erythema observed after C-PDT did not correlate with microcirculatory perfusion and could be a result of inflammation.

Vascular-targeted PDT led to better the long-term tumor response than cellular-targeted PDT. Up to 44% animals showed S91 melanoma tumor regression, lasting at least one year after therapy. V-PDT led to deep and chronic hypoxia, whereas tumor-targeted C-PDT caused transient hypoxia, quickly reversed. **Figure 10A** shows that the pO_2 decrease due to C-PDT correlates with a pO_2 increase in the following 24h. Figure 10B shows a selection of animals where pO_2 level dropped to 0 mmHg at any time after illumination. In this sub-set of data, 80% of the animals treated with V-PDT were cured.

5. Conclusions

Extremely low pO_2 lasting for several days (0-2 mm Hg, i.e. chronic, extreme hypoxia) after vascular-targeted PDT favor long-term tumor responses, in contrast to mild and transient hypoxia, that in tumor-cell targeted PDT lead to strong pO_2 compensatory effects (up to 10-12 mm Hg) and frequent tumor re-growths. V-PDT with F_2BMet in the mouse melanoma model provided significant survival advantage, with a cure rate of 44%. This is a remarkable result for one single PDT treatment of malignant melanoma. V-PDT with F_2BMet is currently in Phase I/II clinical trials.

Acknowledgments

This work was supported by Ministry of Science and Higher Education: Iuventus Plus grant no. IP2011009471 given to JMD. The European Union grants: POIG.02.01.00-12-023/08 and POIG.02.01.00-12-064/08 are acknowledged. Some experiments were also financed by grants nr 2012/05/B/ST5/00389 and nr DEC-2011/03/N/N24/02019 from National Science Center. We thank Dr. Przemysław Płonka for helpful discussions, Dr. Mirosław Zarębski for his help with analysis of the perfusion images, Ms. Dominika Michalczyk-Wetula for animal care, Ms. Magdalena Sroka and Ms. Barbara Pucelik for

the help with measurements. We thank Dr H. Swartz (Darmouth Medical School) for providing LiPc. The EPR spectra were analyzed using the fitting software developed by Dr. Ben Williams and Tom Mathews from the same lab. We thank Luzitin SA for a generous gift of F_2BMet. "LGA, GS and KU declare authoring patents licensed to Luzitin SA, which may be perceived as a potential conflict of interest".

References

[1] Agostinis, P.; Berg, K.; Cengel, K. A.; Foster, T. H.; Girotti, A. W.; Golinick, S. O.; Hahn, S. M.; Hamblin, M. R.; Juzeniene, A.; Kessel, D.; Korbelik, M.; Moan, J.; Mroz, P.; Nowis, D.; Piette, J.; Wilson, B. C.; Golab, J. Photodynamic therapy of cancer: An update. *CA Cancer J. Clin.* **61**: 250-281; 2011.

[2] Schmidt-Erfurth, U.; Hsan, T. Mechanisms of action of photodynamic therapy with verteporfin for the treatment of age-related macular degeneration. *Surv Ophthalmol.* **45**: 195-214; 2000.

[3] Hamblin, M. R.; Hasan, T. Photodynamic therapy: a new antimicrobial approach to infectious disease? *Photochem. Photobiol. Sci.* **3**: 436-450; 2004.

[4] Castano, A. P.; Mroz, P.; Hamblin, M. R. Photodynamic therapy and anti-tumour immunity. *Nat. Rev. Cancer* **6**: 535-545; 2006.

[5] O'Connor, A. E.; Gallagher, W. M.; Byrne, A. T. Porphyrin and nonporphyrin photosensitizers in oncology: Preclinical and clinical advances in photodynamic therapy. *Photochem. Photobiol.* **85**: 1053-1074; 2009.

[6] Phillips, D. Light relief: photochemistry and medicine. *Photochem. Photobiol. Sc.* **9**: 1589-1596; 2010.

[7] Pineiro, M.; Gonsalves, A. M. d. A. R.; Pereira, M. M.; Formosinho, S. J.; Arnaut, L. G. New halogenated phenylbacteriochlorins and their efficiency in singlet-oxygen sensisitzation. *J. Phys. Chem. A* **106**: 3787-3795; 2002.

[8] Chen, Y.; Li, G.; Pandey, R. K. Synthesis of bacteriochlorins and their potential utility in photodynamic therapy (PDT). *Current Org. Chem.* **8**: 1105-1134; 2004.

[9] van Duijnhoven, F. H.; Rovers, J. P.; Engelmann, K.; Krajina, Z.; Purkiss, S. F.; Zoetmulder, F. A. N.; Vogl, T. J.; Terpstra, O. T. Photodynamic therapy with 5,10,15,20-tetrakis(m-hydroxyphenyl) bacteriochlorin for colorectal liver metastases is safe and feasible: Results form a Phase I Study. *Ann. Surg. Oncol.* **12**: 808-816; 2005.

[10] Vakrat-Haglili, Y.; Weiner, L.; Brumfeld, V.; Brandis, A.; Salomon, Y.; Brian Mcllroy; Wilson, B. C.; Pawlak, A.; Rozanowska, M.; Sarna, T.; Scherz, A. The Microenvironment Effect on the Generation of Reactive Oxygen Species by Pd-Bacteriopheophorbide. *J. Am. Chem. Soc.* **127**: 6487-6497; 2005.

[11] Gryshuk, A.; Chen, Y.; Goswami, L. N.; Pandey, S.; Missert, J. R.; Ohulchanskyy, T.; Potter, W.; Prasad, P. N.; Oseroff, A.; Pandey, R. K. Structure-activity relationship among purpurinimides and bacteriopurpurinimides: trifluoromethyl substituent enhanced the photosensitizing efficacy. *J. Med. Chem.* **50**: 1754-1767; 2007.

[12] Silva, E. F. F.; Serpa, C.; Dabrowski, J. M.; Monteiro, C. J. P.; Arnaut, L. G.; Formosinho, S. J.; Stochel, G.; Urbanska, K.; Simoes, S.; Pereira, M. M. Mechanisms of singlet oxygen and superoxide ion generation by porphyrins and bacteriochlorins. *Chem. Eur. J.* **16**: 9273-9286; 2010.

[13] Pereira, M. M.; Monteiro, C. J. P.; Simoes, A. V. C.; Pinto, S. M. A.; Abreu, A. R.; Sa, G. F. F.; Silva, E. F. F.; Rocha, L. B.; Dabrowski, J. M.; Formosinho, S. J.; Simoes, S.; Arnaut, L. G. Synthesis and photophysical characterization of a library of photostable halogenated bacteriochlorins: an access to near infrared chemistry. *Tetrahedron* **66**: 9545-9551; 2010.

[14] Mroz, P.; Huang, Y.-Y.; Szokalska, A.; Zhiyentayev, T.; Janjua, S.; Nifli, A.-P.; Sherwood, M. E.; Ruzié, C.; Borbas, K. E.; Fan, D.; Krayer, M.; Balasubramanian, T.; Yang, E.; Kee, H. L.; Kirmaier, C.; Diers, J. R.; Bocian, D. F.; Holten, D.; Lindsey, J. S.; Hamblin, M. R. Stable synthetic bacteriochlorins overcome the resistance of melanoma to photodynamic therapy. *FASEB J.* **24**: 3160-3170; 2010.

[15] Huang, Y.-Y.; Mroz, P.; Zhiyentayev, T.; Sharma, S. K.; Balasubramanian, T.; Ruzié, C.; Krayer, M.; Fan, D.; Borbas, K. E.; Yang, E.; Kee, H. L.; Kirmaier, C.; Diers, J. R.; Bocian, D. F.; Holten, D.; Lindsey, J. S.; Hamblin, M. R. In vitro photodynamic therapy and quantitative structure-activity relationship studies with stable synthetic near-infrared-absorbing bacteriochlorin photosensitizers. *J. Med. Chem.* **53**: 4018-4027; 2010.

[16] Huang, Y. Y.; Balasubramanian, T.; Yang, E.; Luo, D.; Diers, J. R.; Bocian, D. F.; Lindsey, J. S.; Holten, D.; Hamblin, M. R. Stable synthetic bacteriochlorins for photodynamic therapy: role of dicyano peripheral groups, central metal substitution (2H, Zn, Pd), and Cremophor EL delivery. *ChemMedChem* **7**: 2155-2167; 2012.

[17] Kozyrev, A.; Ethirajan, M.; Chen, P.; Ohkubo, K.; Robinson, B. C.; Barkigia, K. M.; Fukuzumi, S.; Kadish, K. M.; Pandey, R. K. Synthesis, photophysical and electrochemistry of near-IR absorbing bacteriochlorins related to bacteriochlorophyll a. *J. Org. Chem.* **77**: 10260-10271; 2012.

[18] Arnaut, L. G. Design of porphyrin-based photosensitizers for photodynamic therapy. *Adv. Inorg. Chem.* **63**: 187-233; 2011.

[19] Dabrowski, J. M.; Urbanska, K.; Arnaut, L. G.; Pereira, M. M.; Abreu, A. R.; Simoes, S.; Stochel, G. Biodistribution and Photodynamic Efficacy of a Water-Soluble, Stable, Halogenated Bacteriochlorin against Melanoma. *ChemMedChem* **6**: 465-475; 2011.

[20] Dabrowski, J. M.; Arnaut, L. G.; Pereira, M. M.; Urbanska, K.; Simões, S.; Stochel, G.; Cortes, L. Combined effects of singlet oxygen and hydroxyl radical in photodynamic therapy with photostable bacteriochlorins: Evidence from intracellular fluorescence and increased photodynamic efficacy in vitro. *Free Radic. Biol. Med.* **52**: 1188-1200; 2012.

[21] Dabrowski, J. M.; Arnaut, L. G.; Pereira, M. M.; Urbanska, K.; Stochel, G. Improved biodistribution, pharmacokinetics and photodynamic efficacy using a new photostable sulfonamide bacteriochlorin. *MedChemComm* **3**: 502-505; 2012.

[22] Yang, E.; Diers, J. R.; Huang, Y.-Y.; Hamblin, M. R.; Lindsey, J. S.; Bocian, D. F.; Holten, D. Molecular electronic tuning of the photosensitizers to enhance

photodynamic therapy: Synthetic dicyanobacteriochlorins as a case study. *Photochem. Photobiol.* **89**: 605-618; 2013.

[23] Arnaut, L. G.; Pereira, M. M.; Dabrowski, J. M.; Silva, E. F. F.; Schaberle, F. A.; Abreu, A. A.; Rocha, L. B.; Barsam, M. M.; Urbanska, K.; Stochel, G.; Brett, C. M. A. Photodynamic Therapy Efficacy Enhanced by Dynamics: The Role of Charge-Transfer and Photostability in the Selection of Photosensitizers. *Chem. Eur. J.* **20**: 1-13; 2014.

[24] Saavedra, R.; Rocha, L. B.; Dabrowski, J. M.; Arnaut, L. G. Modulation of biodistribution, pharmacokinetics and photosensitivity with the delivery vehicle of a bacteriochlorin photosensitizer for photodynamic therapy. *ChemMedChem* **9**: 390-398; 2014.

[25] Tromberg, B.; Orenstein, A.; Kimel, S.; Barker, S. J.; Hyatt, J.; Nelson, J. S.; Berns, M. W. In vivo tumor oxygen tension measurements for the evaluation of the efficiency of photodynamic therapy. *Photochem. Photobiol.* **52**: 375-385; 1990.

[26] Busch, T. M.; Hahn, S. M.; Evans, S. M.; Koch, C. J. Depletion of tumor oxygenation during photodynamic therapy: detection by the hypoxia marker EF3 [2-(2-nitroimidazol-1[H]-yl)-N (3,3,3-trifluoropropyl)acetamide]. *Cancer Res.* **60**: 2636-2642; 2000.

[27] Gross, S. G.; Gilead, A.; Scherz, A.; Neeman, M.; Salomon, Y. Monitoring photodynamic therapy of solid tumors online by BOLD-contrast MRI. *Nat. Med.* **9**: 1327-1332; 2003.

[28] Curnow, A.; Haller, J. C.; Bown, S. G. Oxygen monitoring during 5-aminolaevulinic acid induced photodynamic therapy in normal rat colon. Comparison of continuous and fractionated light regimes. *J. Photochem. Photobiol. B: Biol.* **58**: 149-155; 2000.

[29] Pogue, B. W.; Hasan, T. A theoretical study of light fractionation and dose-rate effects in photodynamic therapy. *Radiat. Res.* **147**: 551-559; 1997.

[30] Zilberstein, J.; Schreiber, S.; Bloemers, M. C. W. M.; Bendel, P.; Neeman, M.; Schechtman, E.; Kohen, F.; Scherz, A.; Salomon, Y. Antivascular Treatment of Solid Melanoma Tumors with Bacteriochlorophyll–serine-based Photodynamic Therapy. *Photochem. Photobiol.* **73**: 257-266; 2001.

[31] Pogue, B. W.; Braun, R. D.; Lanzen, J. L.; Erickson, C.; Dewhirst, M. W. Analysis of the heterogeneity of pO2 dynamics during photodynamic therapy with verteporfin. *Photochem. Photobiol.* **74**: 700-706; 2001.

[32] Zilberstein, J.; Bromberg, A.; Rosenbach-Belkin, V.; Kritzmann, A.; Pfefermann, R.; Salomon, Y.; Scherz, A. Light-dependent oxygen consumption in bacteriochlorophyll-serine-treated melanoma tumors: on-line determination using a tissue-inserted oxygen microsensor. *Photochem. Photobiol.* **65**: 1012-1019; 1997.

[33] Krammer, B. Vascular effects of photodynamic therapy. *Anticancer Res.* **21**: 4271-4277; 2001.

[34] Chen, B.; Pogue, B. W.; Hoopes, P. J.; Hasan, T. Combining vascular and cellular targeting regimes enhances the efficacy of photodynamic therapy. *Int. J. Rad. Oncol. Biol. Phys.* **61**: 1216-1226; 2005.

[35] Fuchs, J.; Thiele, J. The role of oxygen in cutaneous photodynamic therapy. *Free Radic. Biol. Med.* **24**: 835–847; 1998.

[36] Pogue, B. W.; Paulsen, K. D.; O'Hara, J. A.; Wilmot, C. J.; Swartz, H. M. Estimation of oxygen distribution in RIF-1 tumors by diffusion model-based interpretation of pimonidazole hypoxia and eppendorf measurements. *Radiat. Res.* **155**: 15-25; 2001.

[37] Wang, H.-W.; Putt, M. E.; Emanuele, M. J.; Shin, D. B.; Glatstein, E.; Yodh, A. G.; Busch, T. M. Treatment-induced changes in tumor oxygenation predict photodynamic therapy outcome. *Cancer Res.* **64**: 7553-7561; 2004.

[38] Ferrario, A.; von Tiehl, K. F.; Rucker, N.; Schwarz, M. A.; Gill, P. S.; Gomer, C. J. Antiangiogenic treatment enhances photodynamic therapy responsiveness in a mouse mammary carcinoma. *Cnacer Res.* **60**: 4066-4069; 2000.

[39] Uehara, M.; Inokuchi, T.; Sano, K.; ZuoLin, W. Expression of vascular endothelial growth factor in mouse tumours subjected to photodynamic therapy. *Eur. J. Cancer* **37**: 2111-2115; 2001.

[40] Tatum JL, Kelloff GJ, Gillies RJ, Arbeit JM, Brown JM, et al. (2006) Hypoxia: importance in tumor biology, noninvasive measurement by imaging, and value of its measurement in the management of cancer therapy. Int J Radiat Biol 82: 699–757.

[41] He, G.; Shankar, R. A.; Chzhan, M.; Samouilov, A.; Kuppusamy, P.; Zweier, J. L. Noninvasive measurement of anatomic structure and intraluminal oxygenation in the gastrointestinal tract of living mice with spatial and spectral EPR imaging. *Proc. Natl. Acad. Sci. USA* **96**: 4586–4591; 1999.

[42] Swartz, H. M.; Clarkson, R. B. The measurement of oxygen in vivo using EPR techniques. *Phys. Med. Biol.* **43**: 1956-1975; 1998.

[43] Halpern, H. J.; Yu, C.; Peric, M.; Barth, E.; Grdina, D. J.; Teicher, B. A. Oxymetry deep in tissues with low-frequency electron paramagnetic resonance. *Proc. Natl. Acad. Sci. USA* **91**: 13047–13051; 1994.

[44] Elas, M.; Williams, B. B.; Parasca, A.; Mailer, C.; Pelizzari, C. A.; Lewis, M. A.; River, J. N.; Karczmar, G. S.; Barth, E. D.; Halpern, H. J. Quantitative Tumor Oxymetric Images From 4D Electron Paramagnetic Resonance Imaging (EPRI): Methodology and Comparison With Blood Oxygen Level-Dependent (BOLD) MRI. *Magn. Reson. Med.* **691**: 682–691; 2003.

[45] Allez, B. E. G.; Gallez, B.; Mader, K. Accurate and sensitive measurements of pO2 in vivo using low frequency EPR spectroscopy: how to confer biocompatibility to the oxygen sensors. *Free Radic. Biol. Med.* **29**: 1078–1084; 2000.

[46] Hou, H.; Lariviere, J. P.; Demidenko, E.; Gladstone, D.; Swartz, H.; Khan, N. Repeated tumor pO(2) measurements by multi-site EPR oximetry as a prognostic marker for enhanced therapeutic efficacy of fractionated radiotherapy. *Radiother. Oncol.* **91**: 126–131; 2009.

[47] Dabrowski, J. M.; Pereira, M. M.; Arnaut, L. G.; Monteiro, C. J. P.; Peixoto, A. F.; Karocki, A.; Urbanska, K.; Stochel, G. Synthesis, photophysical studies and anticancer activity of a new halogenated water-soluble porphyrin. *Photochem. Photobiol.* **83**: 897-903; 2007.

[48] Dabrowski, J. M.; Arnaut, L. G.; Pereira, M. M.; Monteiro, C. J. P.; Urbanska, K.; Simões, S.; Stochel, G. New halogenated water-soluble chlorin and bacteriochlorin as phototable PDT sensitizers: synthesis, spectroscopy and photophysics and in vitro photosensitizing efficacy. *ChemMedChem* **5**: 1770-1780; 2010.

[49] Dunn, J. F.; Swartz, H. M. In vivo electron paramagnetic resonance oximetry with particulate materials. *Methods* **30**: 159-166; 2003.

[50] Liu, K. J.; Gast, P.; Moussavi, M.; Norby, S. W.; Vahidi, N.; Walczak, T.; Wu, M. X.; Swartz, H. M. Lithium phthalocyanine: a probe for electron paramagnetic resonance oximetry in viable biological systems. *Proc. Natl. Acad. Sci. USA* **90**: 5438-5442; 1993.

[51] Dabrowski, J. M.; Krzykawska, M.; Arnaut, L. G.; Pereira, M. M.; Monteiro, C. J. P.; Simões, S.; Urbanska, K.; Stochel, G. Tissue Uptake Study and Photodynamic Therapy of Melanoma-Bearing Mice with a Nontoxic, Effective Chlorin. *ChemMedChem* **6**: 1715-1726; 2011.

[52] Silva, E. F. F.; Schaberle, F. A.; Monteiro, C. J.; Dąbrowski, J. M.; Arnaut, L. G. The challenging combination of intense fluorescence and high singlet oxygen quantum yield in photostable chlorins – a contribution to theranostics. *Photochem. Photobiol. Sci.* **12**: 1187-1192; 2013.

[53] Pogue, B. W.; O'Hara, J. A.; Goodwin, I. A.; Wilmot, C. J.; Fournier, G. P.; Akay, A. R.; Swartz, H. Tumor PO(2) changes during photodynamic therapy depend upon photosensitizer type and time after injection. *Comp Biochem Physiol A Mol Integr Physiol.* **132**: 177-184; 2002.

[54] Sitnik, T. M.; Hampton, J. A.; Henderson, B. W. Reduction of tumour oxygenation during and after photodynamic therapy in vivo: effects of fluence rate. *Br. J. Cancer* **77**: 1386-1394; 1998.

[55] Preise, D.; Scherz, A.; Salomon, Y. Antitumor immunity promoted by vascular occluding therapy: Lessons from vascular-targeted photodynamic therapy (VTP). *Photochem. Photobiol. Sci.* **10**: 681-688; 2011.

[56] Leach, R. M.; Treacher, D. F. Oxygen transport — 2. Tissue hypoxia. *BMJ* **317**: 1370-1373; 1998.

Figure captions

Scheme 1. Molecular structure of 5,10,15,20-tetrakis(2,6-difluoro-3-N-methylsulfamoylphenyl) bacteriochlorin (F_2BMet).

Scheme 2. Experimental setup for Electron Paramagnetic Resonance (left) and Laser Doppler Perfusion Imaging (right) measurements. pO_2 was determined from the EPR spectrum linewidth of the solid state spin probe LiPc. Blood flow LDPI measurements were performed at stable ambient temperature of 38 °C.

Fig. 1. Absorption and fluorescence spectra of F_2BMet in PBS:Cremophor EL:ethanol vehicle (7.5 μM). The fluorescence was obtained with excitation at 507 nm.

Fig. 2. Microcirculatory blood perfusion in legs with tumor. (A) Representative black and white LDPI image with marked tumor area where the blood perfusion measurement was taken. (B-G) Examples of histograms of blood perfusion values in all pixels of the measured area, showing the high variety of distributions of blood perfusion values (wide, narrow, single- or double peak) in untreated tumors.

Fig. 3. Representative images showing superficial microcirculatory blood flow in the leg. S91 tumor before, 15 min, 3 h and then several time points after V-PDT (A, B) or C-PDT (C, D). Blood perfusion in the images was measured in the areas marked (1) *vena sapiena lateralis*, (2) tumor or post-tumor area and (3) skin lesion or scab. (E) Untreated large tumor (F) normal untreated leg without tumor. (3.1) Kinetics of blood perfusion after V-PDT in the same animals as in (A) and (B). (3.2) Kinetics of blood perfusion after C-PDT in the same animals as in (C) and (D). Blood perfusion was expressed as the ratio of blood perfusion measured in the treated leg to the blood perfusion of the contralateral leg in the same animal, with SD indicated.

Fig. 4. Oxymetric probe localization within the tumor and EPR pO_2 measurements (mean values with SD) for representative S91 tumors after V- PDT (A, B) and C-PDT (C, D) are shown. LiPc crystal position in each tumor was monitored: (A) LiPc was in the upper part of the tumor. (B) LiPc was in the upper part of the tumor, slightly smaller than in (A). (C) LiPc crystal was in the lower part of the tumor. (D) LiPc was in the middle of the tumor.

(4.1) pO_2 kinetics of tumors (A) and (B) treated with V-PDT. (4.2) Strongly individualized pO_2 responses to therapy observed after C-PDT.

Fig. 5. The kinetics of mean pO_2 (squares, left axis) and blood flow (dots, right axis) in S91 tumors. Time origin was selected as the moment of irradiation (arrowhead). Tumors were treated with: (A) V-PDT, (B) C-PDT, (C) Light only, vehicle injection. (D) PS injection, no light. In V-PDT the measurements were discontinued when perfusion returned to normal tissue level. N is the initial number of animals in the group. Most points were significantly different between C-PDT and V-PDT, whereas controls did not differ significantly. Statistical significance was determined using Welch t-test ($p<0.05$).

Fig. 6 VEGF level in tumor homogenates collected 24 h after treatment. Number of animals in light, untreated and dark controls: N=3; in V-PDT: N=4; in C-PDT: N=5. From a single animal two samples were taken. Statistical significance was tested using Mann-Whitney U test, * $p< 0.05$, # $p< 0.09$.

Fig. 7. Kaplan Meier plot for animals with S91 tumors treated with V-PDT (N=13), C-PDT (N=16), and dark (N=7) and light control (N=9). Percentage of animals with tumor volume less than 400 mm^3 is shown. Animals with tumors > 400 mm^3 were sacrificed. Differences between all groups were statistically significant as determined by Wilcoxon (Gehan) test (p=0.004-0.011), except for light and dark control (p=0.915). Photographs of a representative S91 tumor growing in the leg before and after V-PDT (upper) and C-PDT (lower). Tumor outline is marked in white in the first photograph. Erythema and edema are clearly recognized after the treatment.

Fig. 8. Generation of ROS in PBS assessed by the fluorescence of products generated by APF (selective towards hydroxyl radicals) or by SOSG (specific or singlet oxygen). The concentrations of the probes were initially 10 μM and F_2BMet was 5 μM in each well.

Fig. 9. (A) Percentage of animals with erythema of the skin of the PDT-treated leg on day 3 after the therapy. Erythema intensity was scaled from minimal to maximal as 0.5-2, with 0 meaning no skin redness. The statistical significance was tested using Fischer exact test. (B) Edema of the PDT-treated legs, expressed as % of initial tumor volume (mean value with SD). Tumors treated with light and vehicle only increased their volume

due to tumor growth (striped), whereas treated tumor volume drastically increased after treatment and then decreased in time. Star shows statistical significance (t-test, $p<0.05$) between C-PDT and V-PDT. (C) Relative blood flow in *vena sapiena lateralis* (leg with the tumor/leg without the tumor) showing lack of correlation with edema in (B). * $p<0.05$.

Fig. 10. (**A**) ΔpO_2 (before – immediately after) vs ΔpO_2 (24h – 15 min) for V-PDT (♦) and C-PDT (▲), from the data in Fig. 3. (**B**) Kaplan Meier plot for animals with S91 tumors treated with V-PDT (Wilcoxon (Gehan) test, $p=0.055$, N=2 (>0 mmHg), N=6 (=0 mm Hg)), showing 80% cure rate of animals in which the pO_2 level dropped to 0 mmHg at any time after illumination**.**

Scheme 1

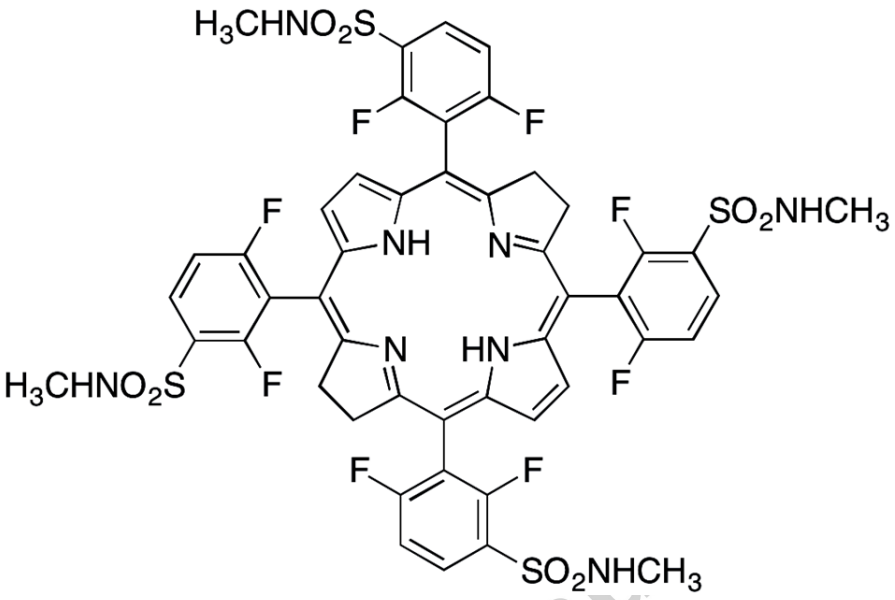

Scheme 2

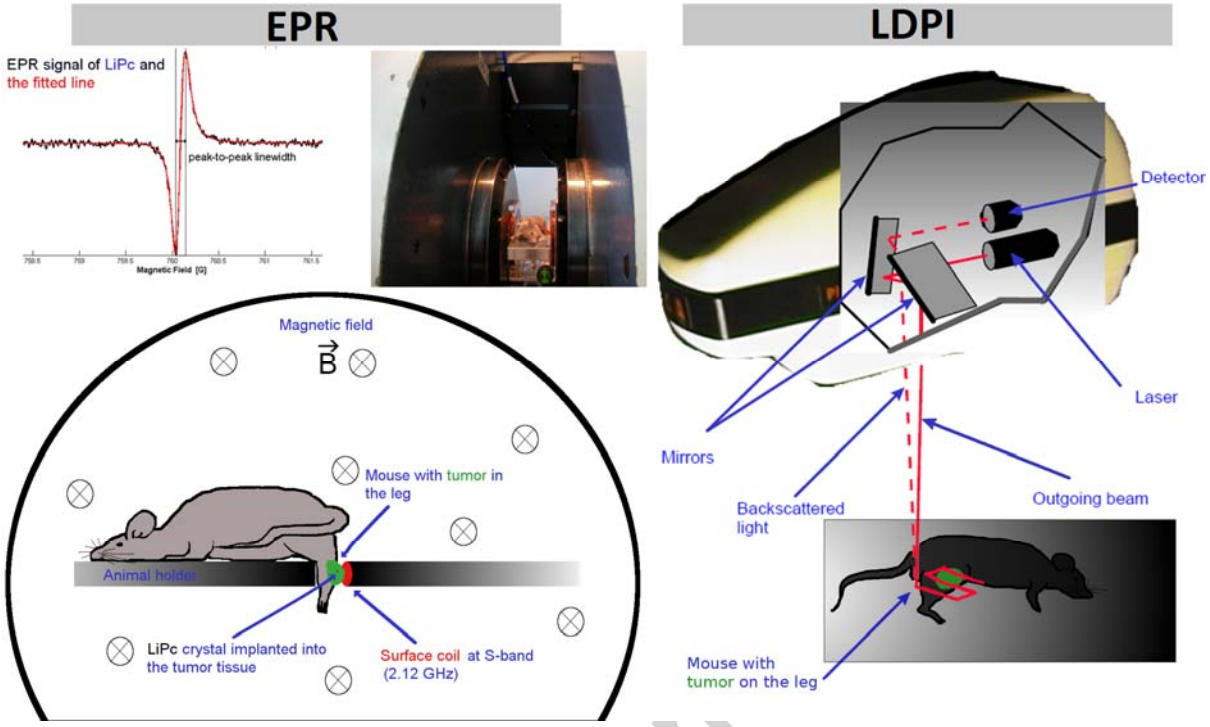

Table 1. Concentration of F_2BMet in various organs and tissues, in units µg F_2BMet / g of tissue, 15 min and 72 h after the iv administration of 2 mg/kg in the formulation Cremophor:ethanol:NaCl 0.9% (1:1:98) with 5 animals per group.

Organs/Tissues	15 minutes after injection		72 hours after injection	
	F_2BMet µg/g tissue	SEM	F_2BMet µg/g tissue	SEM
Blood	11.4	0.723	0.71	0.048
Tumor	2.55	0.532	5.42	0.903
Muscle	1.22	0.161	1.27	0.087
Skin	1.17	0.045	1.44	0.072
Liver	2.99	0.129	1.71	0.061
Kidneys	2.52	0.178	1.58	0.055
Spleen	4.97	0.409	3.11	0.227
Intestine	1.24	0.176	1.50	0.163
Lungs	2.86	0.317	1.75	0.219
Heart	2.25	0.132	1.51	0.076

Table 2. Tumor-to-tissue ratios of F_2BMet in surrounding tissues such as muscle and skin after the iv administration of 2 mg/kg in the formulation cremophor:ethanol:NaCl 0.9% (1:1:98).

Organs	15 minutes after injection	72 hours after injection
	F_2BMet µg/g tissue	F_2BMet µg/g tissue
Muscle	2.1	4.3
Skin	2.2	3.8

Figure 1

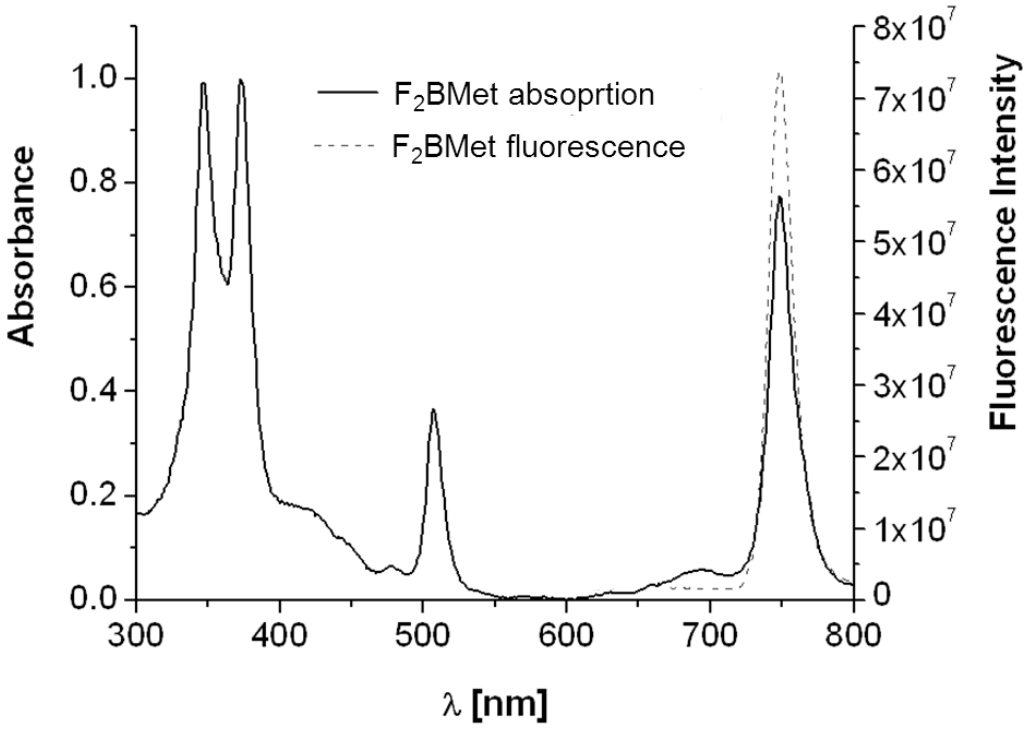

Figure 2

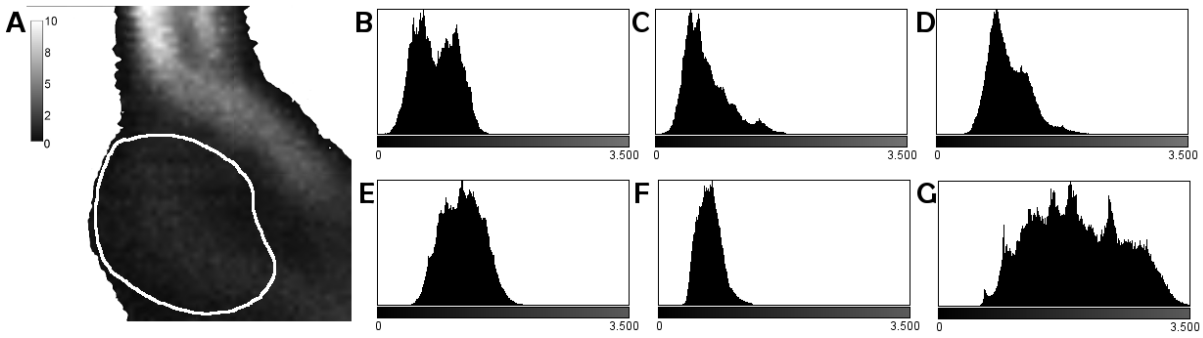

Figure 3

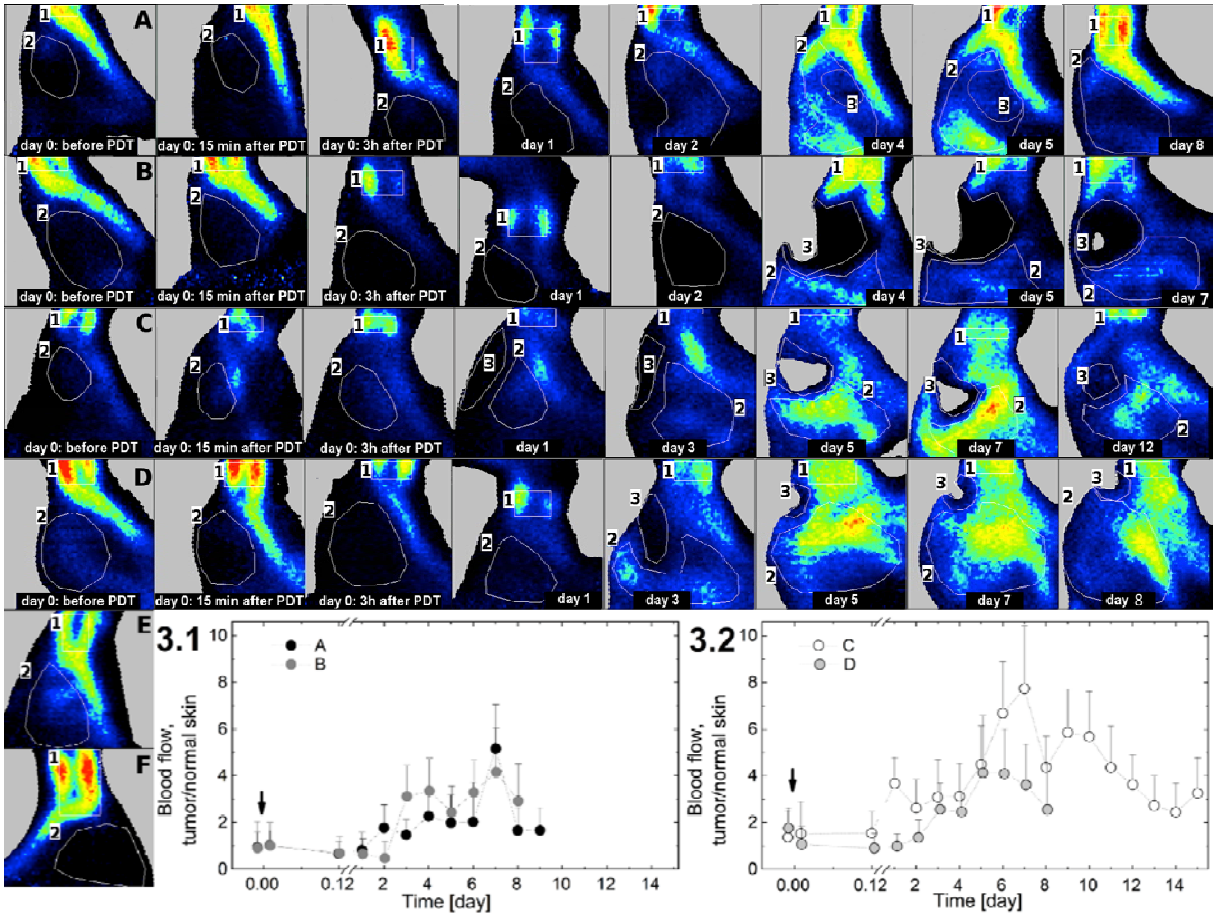

Figure 4

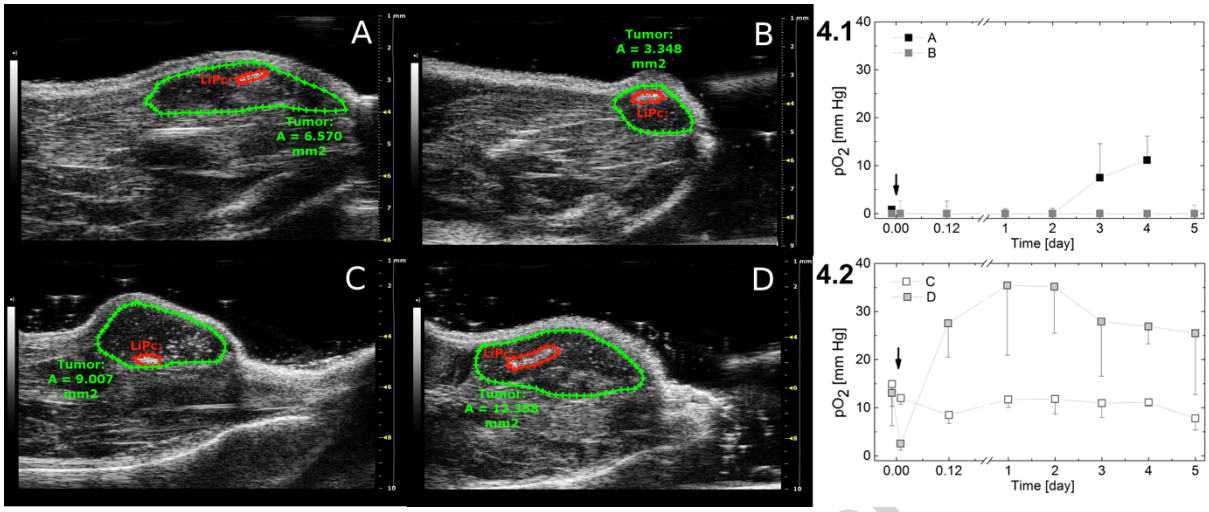

Figure 5

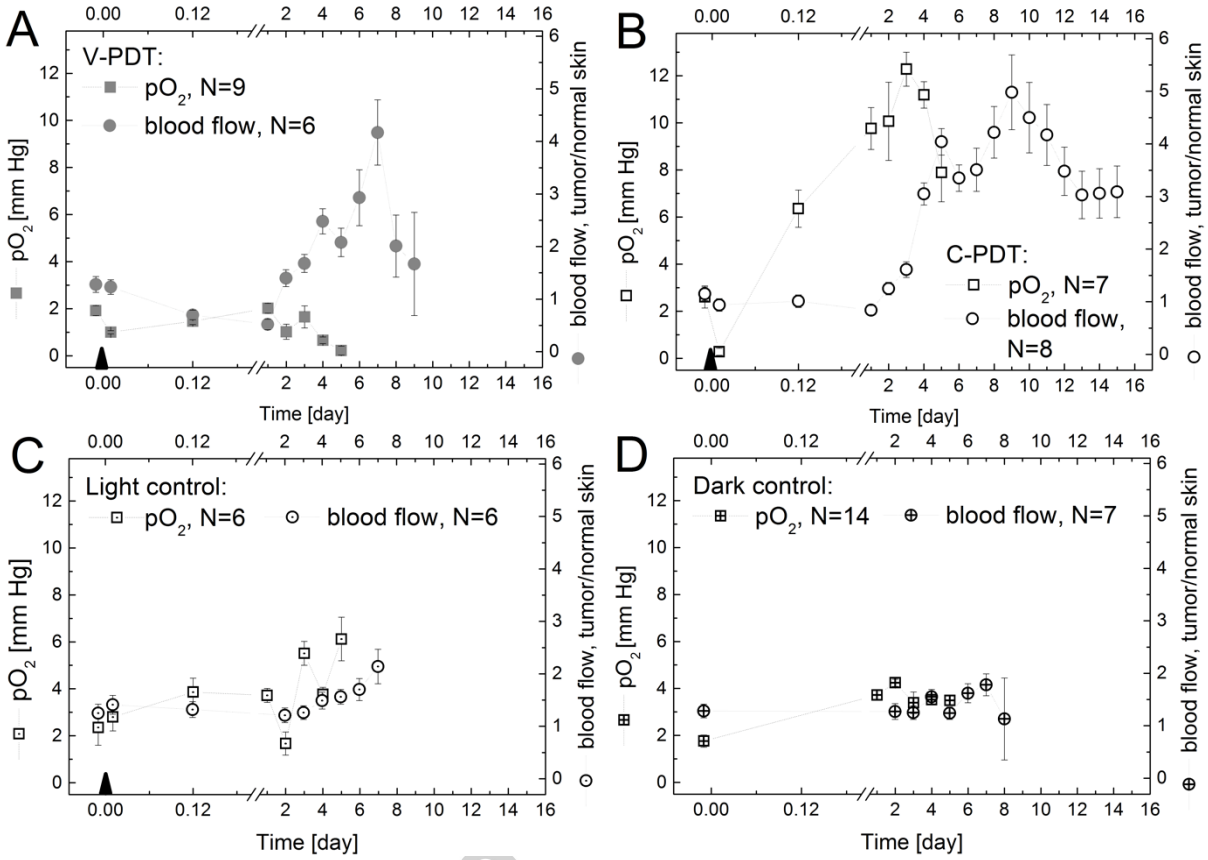

Figure 6

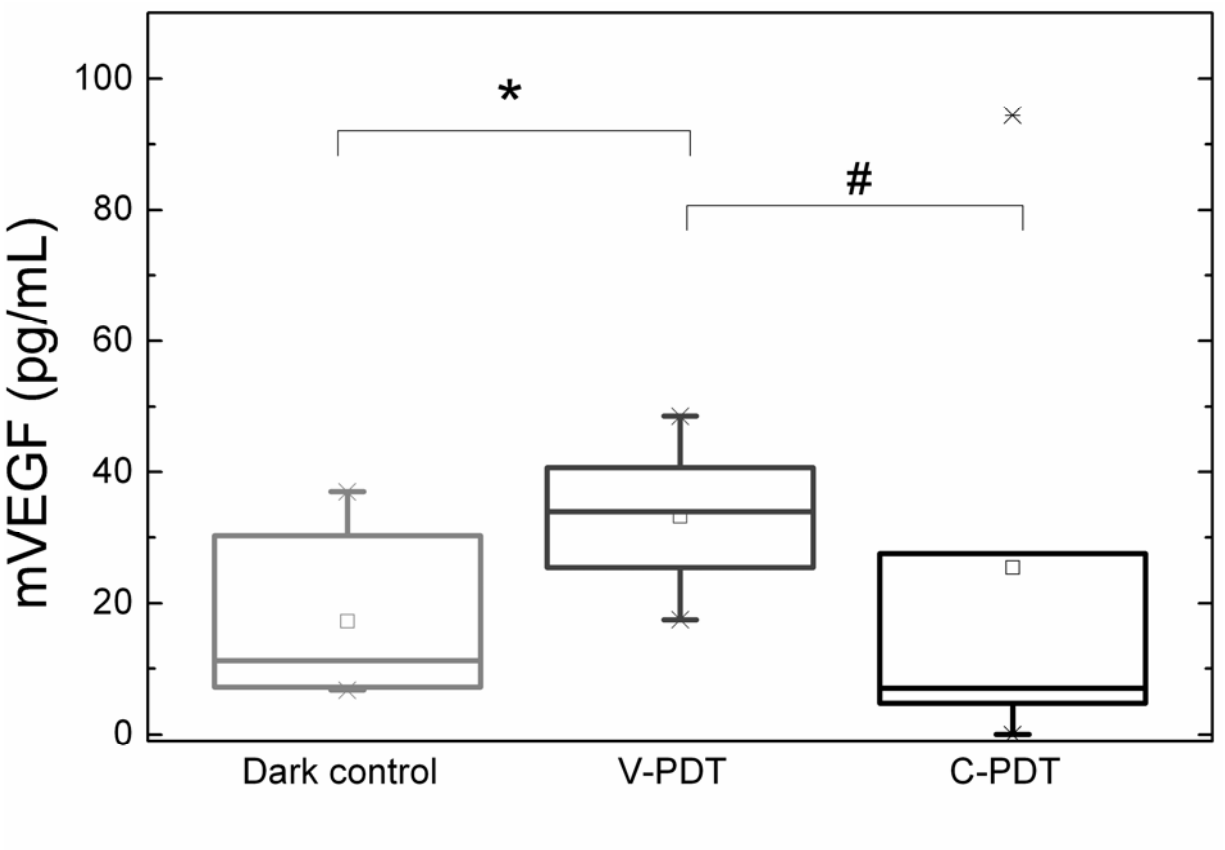

Figure 7

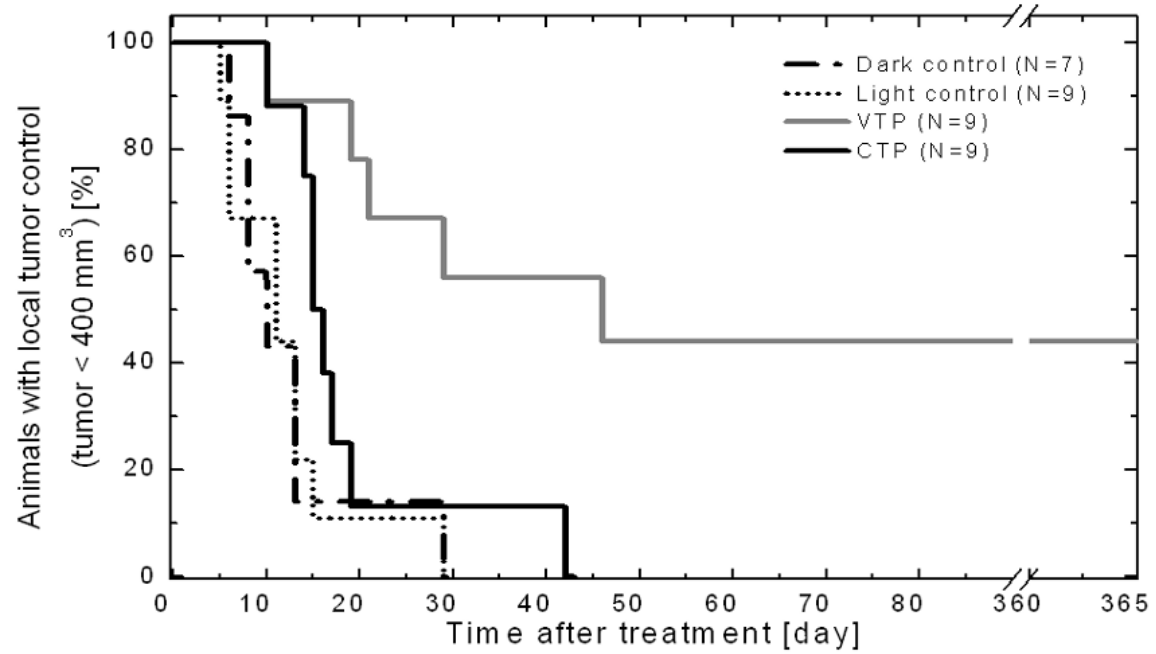

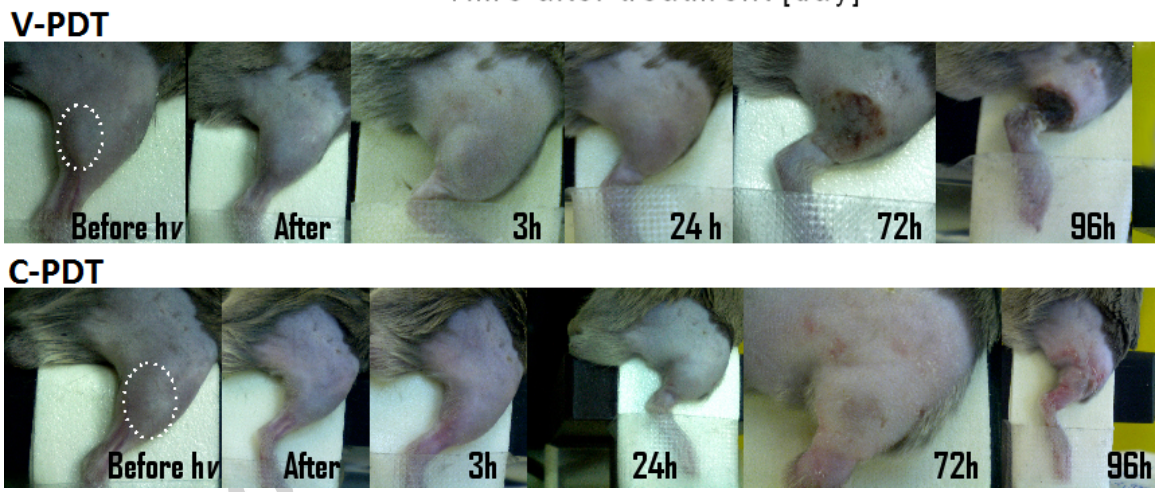

Figure 8

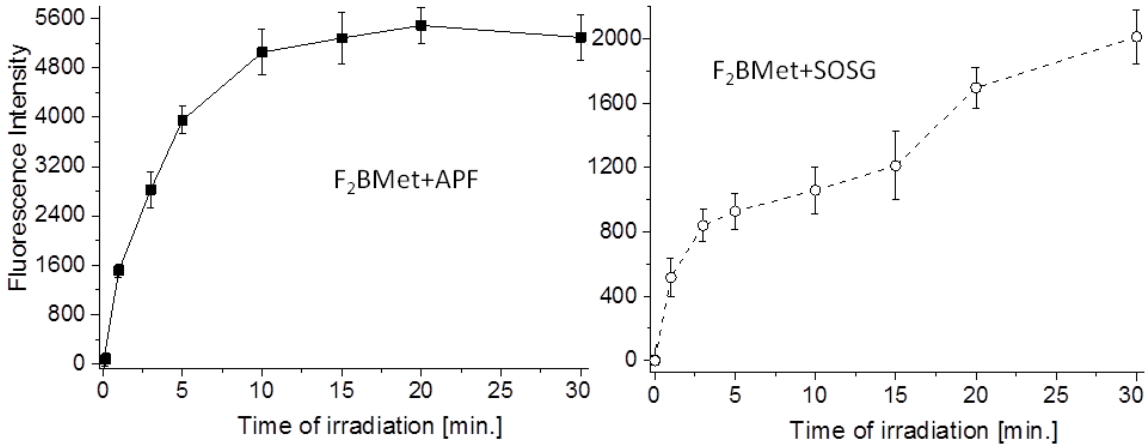

Fig. 9.

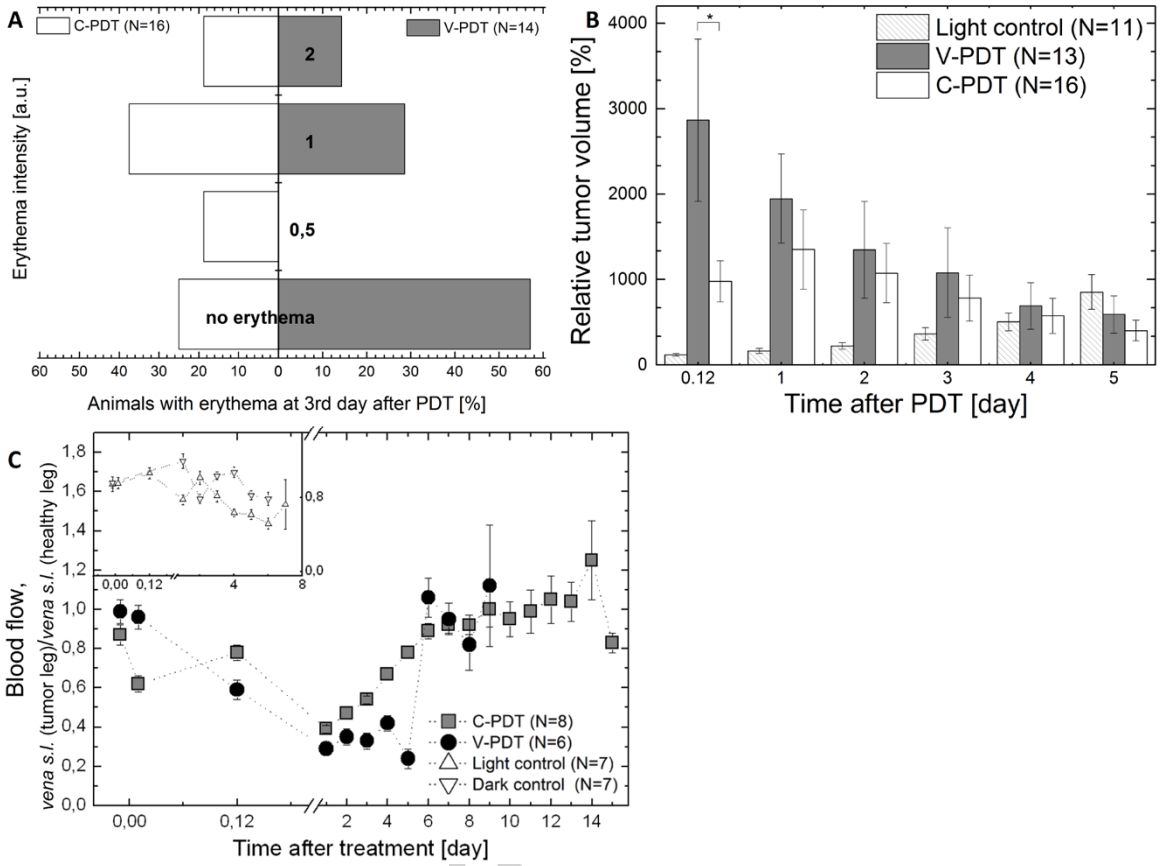

Figure 10

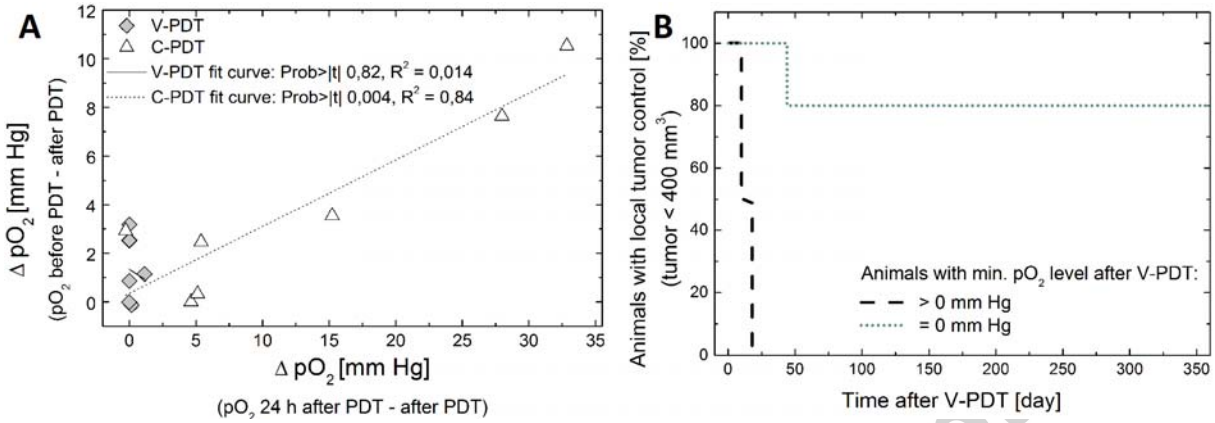

Highlights

F_2BMet generates both singlet oxygen and hydroxyl radicals under NIR irradiation

EPR oximetry informs on hypoxia and Laser Doppler on blood perfusion after PDT

Persistent local hypoxia after PDT correlates with the cure of S91 melanoma tumors

Vascular-PDT induces chronic, extreme hypoxia and is more curative than cellular-PDT

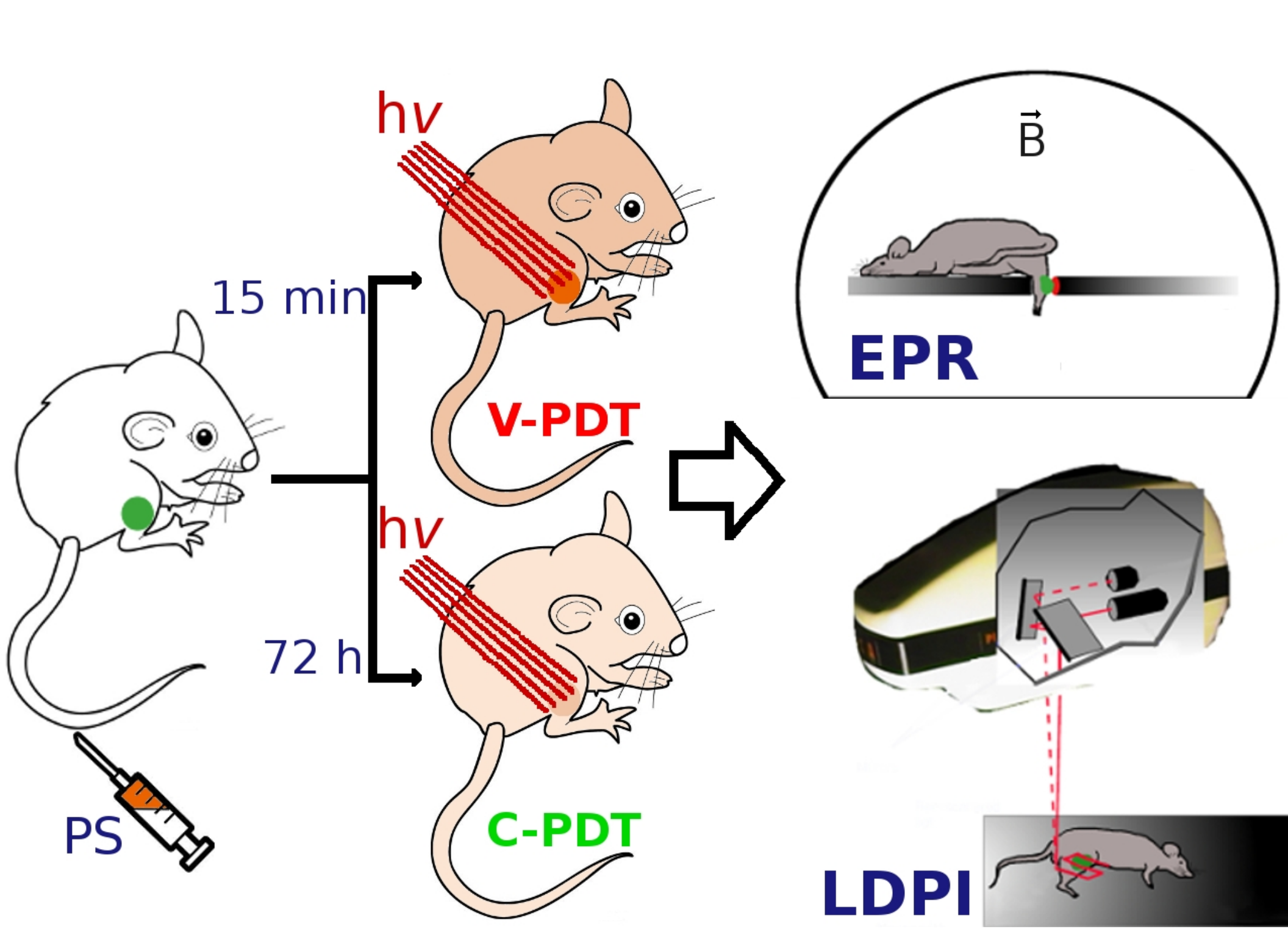
hν
15 min
V-PDT
hν
72 h
C-PDT
PS
B
EPR
LDPI